Soft Matter

Dynamic Article Links

Cite this: *Soft Matter*, 2011, **7**, 11319

www.rsc.org/softmatter

COMMUNICATION

# Growth strain-induced wrinkled membrane morphology of white blood cells

**Lifeng Wang,*[ab] Carlos E. Castro[ac] and Mary C. Boyce*[a]**

***Received 27th August 2011, Accepted 26th October 2011***
**DOI: 10.1039/c1sm06637d**

**The membranes of white blood cells possess a highly corrugated or wrinkled surface topology. This topology provides excess surface area which serves as a reservoir for membrane expansion during osmotic swelling and for membrane mediated events such as adhesion and sensing. We explore and model the dynamic development of the wrinkled morphology to arise from buckling instabilities triggered by the deformation mismatch between the membrane and the cytoskeleton during membrane growth. In particular, we examine the formation of the wavelengths and amplitudes of the wrinkled topology during the large deformations of the membrane growth, which lead to the experimentally observed spicule-like character of the topology. The anisotropic nature of the membrane structure and mechanical behavior, in particular the high stiffness resisting surface area change which provides a high biaxial bending stiffness of the membrane, are found to play an important role in topology development.**

A key component of a biological cell is the cell membrane, composed of a lipid bilayer anchored to the underlying cytoskeleton *via* protein mediated interactions. Motile cells are often observed to change their shape in cell polarization, pseudopod formation, phagocytosis and chemotaxis.[1] During these functional deformations, the cell membrane surface area expands 30%–100%.[2,3] Since a plasma membrane can experience only small strain (~5%) prior to rupture,[4] it has been argued that the observed surface area expansion must be achieved by integration of lipids into the outer membrane or by the unfolding of surface wrinkles.[1,5] White blood cells in particular, specifically neutrophils and B cells, are observed to possess a wrinkled surface morphology in the passive state (see Fig. 1).[3,6] Here we focus on the wrinkled topology of B cell membranes. The primary role of B cells is to detect foreign antigens in the body. The wrinkled topology of the B cell membrane facilitates the large deformations of the membrane required for several stages of its physiological function, in particular migration, antigen detection, and differentiation. For example, when probing lymphoid tissues for antigens, the B cell membrane may spread or crawl along the tissue surface to cover an area larger than the diameter of the cell.[7] Upon detection of antigens, B cells undergo differentiation into Plasma cells which may secrete up to thousands of antibodies per second.[8] To achieve this massive antibody production, B cells undergo a large volumetric expansion from a typical diameter of ~4–6 μm up to a diameter of ~8–12 μm, requiring a surface area expansion of ~100–400%. Since the allowed maximum areal strain of the lipid bilayer is much smaller than the necessary expansion, it has been postulated that B cell membranes utilize their wrinkled topology as a reservoir of surface area to achieve this surface area increase.[9] In this paper, we show that the wrinkled morphology of the white blood cell membrane can result from buckling instabilities which occur during membrane growth. The wrinkled membrane topology enables the necessary physiological large volumetric changes in the cell without rupturing the lipid bilayer.

Fig. 1b shows a naive B cell (a B cell that has not yet encountered its corresponding antigen), which has an extensively wrinkled surface topology. The cell membrane is comprised of a relatively stiff phospholipid bilayer connected to the relatively softer cytoskeleton through various transmembrane proteins as shown in Fig. 1c. We postulate that the underlying mechanism of the wrinkled morphology is a buckling instability in the membrane that occurs during membrane growth by addition of lipids. During growth, the mismatch between the growth rate of the membrane surface area and the volumetric growth of the cytoskeleton results in a compressive hoop stress in the membrane. Once a critical compressive stress is reached, buckling of the membrane is energetically favored over continued uniform

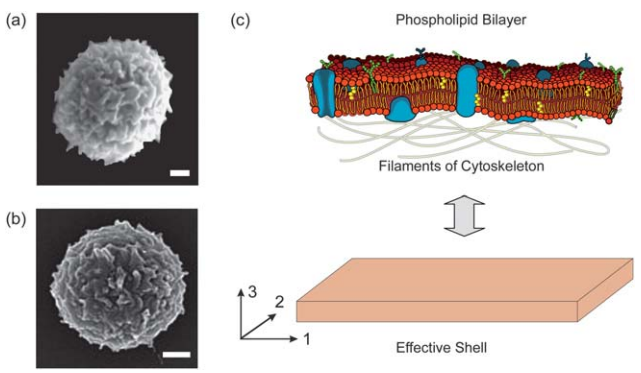


**Fig. 1** White blood cells with wrinkled membrane morphology. (a) Scanning electron micrograph of a human neutrophil.[5] (b) Scanning electron micrograph of a human B-Cell.[7] Scale bar: 1 μm. (c) Illustration of a white blood cell membrane showing lipid bilayer structure, which is modeled as an effective shell.

[a]*Department of Mechanical Engineering, Massachusetts Institute of Technology, Cambridge, MA 02139, USA. E-mail: lifwang@clarkson.edu; mcboyce@mit.edu*
[b]*Department of Civil & Environmental Engineering, Clarkson University, Potsdam, NY 13699, USA*
[c]*Department of Mechanical and Aerospace Engineering, The Ohio State University, Columbus, OH 43210, USA*

circumferential compression of the membrane. The membrane buckles at a wavelength that results in the lowest total energy for the system. This basic phenomenon is well known in classic mechanics as the "buckling of a thin structure (a beam, a plate, a shell) on an elastic foundation". Similar buckling phenomena have recently been studied extensively for thin films on compliant substrates[10–15]and spheroidal core/shell structures[16–19] with various triggering mechanisms of buckling, including prestrain, thermal expansion mismatch, shrinkage or growth rates mismatch. The wavelength of the individual wrinkles is determined by the film mechanical properties and thickness and the substrate mechanical properties.[14,18]For the case of a thin film on a planar substrate, the buckling patterns appear as stripes, herringbones, and labyrinths, depending on the initial constraint conditions.[14] For the case of a thin film on a curved substrate, especially on a closed substrate, the curvature and the topological constraint can play a role in the buckling pattern.[16]

The cell membrane has been modeled as an effective structural shell (see Fig. 1c) possessing elastic Young's modulus $E$, Poisson's ratio $\nu$, and thickness $t$. This approach has been successfully used to predict the deformation mechanics of the human red blood cell.[20] Here, our first set of simulations take the membrane and the cytoskeleton to be homogeneous and isotropic elastic materials with membrane Young's modulus $E_m$, Poisson's ratio $\nu_m$, and thickness $t$; and with cytoskeleton Young's modulus $E_c$, Poisson's ratio $\nu_c$, and the cell radius is $a$. Typically, $E_m = \sim 100$kPa, and $E_c = \sim 1$kPa.[21] For the purposes of this study, the presence of a nucleus can be neglected since the cytoskeleton depth is 100 times larger than the membrane thickness. Furthermore, considering the thickness of a cell membrane 4∼10 nm[21] and the cell radius $a$ is 3∼15μm, the geometry ratio $a/t$ is large and the core curvature is expected to have minimal effect on the critical condition of membrane buckling. Under an equibiaxial stress/strain condition, the critical wavelength and critical strain associated with buckling of an elastic film (membrane) on a compliant substrate (cytoskeleton) can be given as[11,14,18]

$$\lambda_{crit} = 2\pi t\left(\frac{3E_c(1-\nu_m{}^2)}{E_m(1-\nu_c{}^2)}\right)^{-1/3}. \quad (1)$$

$$\varepsilon_{crit} = \frac{1}{4(1+\nu_m)}\left(\frac{3E_c(1-\nu_m{}^2)}{E_m(1-\nu_c{}^2)}\right)^{2/3} \quad (2)$$

The wavelength is seen to scale with $(E_c(1-\nu_m^2)/E_m(1-\nu_c^2))^{-1/3}$, linearly with membrane thickness $t$, and is independent of the cell radius $a$. This is confirmed by the numerical simulation results later.

Buckling patterns are further studied numerically using 3D nonlinear finite element analysis (FEA) with ABAQUS/Explicit. Initial buckling modes are determined using FEA based on an eigenanalysis under external pressure loading. Initial imperfections are then introduced in the form of a very small amplitude of the critical mode and the membrane is then subjected to growth *via* a simulated areal expansion while retaining the core at constant volume. This leads to the radial mismatch condition between the core and the membrane that triggers the buckling of the membrane. The post-buckling analysis is then conducted up to 30% membrane strain.

Fig. 2a depicts the evolution of membrane surface morphology during membrane area growth where typical values are used for material properties ($E_m = \sim 100$ kPa, and $E_c = \sim 1$ kPa, $\nu_m = \nu_c = 0.49$, and $a = 2500$ nm and $t = 5$ nm).[21–25] Above the critical condition, a random dent-like pattern first appears in the membrane and soon transforms into collections of parallel wrinkles. This transformation occurs because maintaining the dent-like pattern requires extensive areal stretching under large deformations and hence is not energetically favorable during the post-buckling stages. The length of the parallel wrinkles is observed to be ∼2–3 times that of the wavelength. As the membrane continues to grow, the buckle amplitude increases and the wrinkles further break into a more disordered herringbone-type of zigzag pattern. The final labyrinth patterns after a 56% area increase of the membrane provide the lowest bending energy configuration at large growth strain as shown in Fig. 2b where strain energy is concentrated at the peaks and valleys of the wrinkles, forming the spicule-like sharp folds commonly observed on white blood cells. The substrate (or cytoskeleton) energy contribution is due to the penetration strain into the substrate by a thin layer where the depth scales with the wavelength. This agrees well with the case of a cylindrical shell/core structure.[18] The interplay between the cytoskeleton and membrane energy contributions is shown in Fig. 2c. At small deformation, the energy of both the cytoskeleton and the membrane increase in a quadratic manner depending on the growth strain ($\varepsilon_{growth}$) of the membrane, where the total energy consists of the stretching strain energy of the membrane and the volumetric strain energy of the core. After the critical condition, both energies increase linearly where the bending strain energy becomes dominant in the membrane and shear strain energy is dominant in the cytoskeleton. Hence, the wrinkled morphology is clearly energetically favored over the smooth surface since the energy of the smooth surface would have continued to increase quadratically. During membrane growth, the diameter of the cell remains nearly unchanged and the surface area expands. This indicates the wrinkled cell surface could serve as a large reservoir for providing membrane area expansion during volumetric growth of the cell by unfolding these wrinkles.[3,9,26]

The curvature is expected to have a negligible effect on the post-buckling morphology due to large geometry ratio $a/t$. Here, the simulation results for the surface morphologies of a spherical membrane and a planar membrane with the same material properties and membrane thickness ($E_m/E_c = 100$, $\nu_m = \nu_c$, $t = 5$ nm) are compared. The excellent similarity of the wrinkled patterns in Fig. 3a indicates no apparent curvature-dependence of the morphology. The critical wavelength (the width) of an individual wrinkle of these two cases is approximately identical, ∼ 100 nm, and agrees well with the theory prediction from eqn (1). Considering the membrane thickness is constant and $\nu_m = \nu_c$, the critical wavelength is seen to scale with $(3E_m/E_c)^{1/3}$. Fig. 3b shows the critical wavelength as a function of modulus ratio of the membrane and the substrate at a given membrane thickness of 5 nm. The wavelengths of both spherical membrane and planar membrane are shown to be an exponential function of $E_m/E_c$. The numerical results are in agreement with theoretical prediction, indicating the capability of analytical solution for predicting wavelength of the membrane on both spherical and planar substrates. For a planar thin film on a compliant substrate, the amplitude for the buckling is obtained as[11,14]

$$A = t\sqrt{\frac{\varepsilon_{growth}}{\varepsilon_{crit}} - 1} \quad (3)$$

Fig. 3c shows the amplitude of buckled membrane as a function of growth strain. When the growth strain is relatively small (<12%), the

 

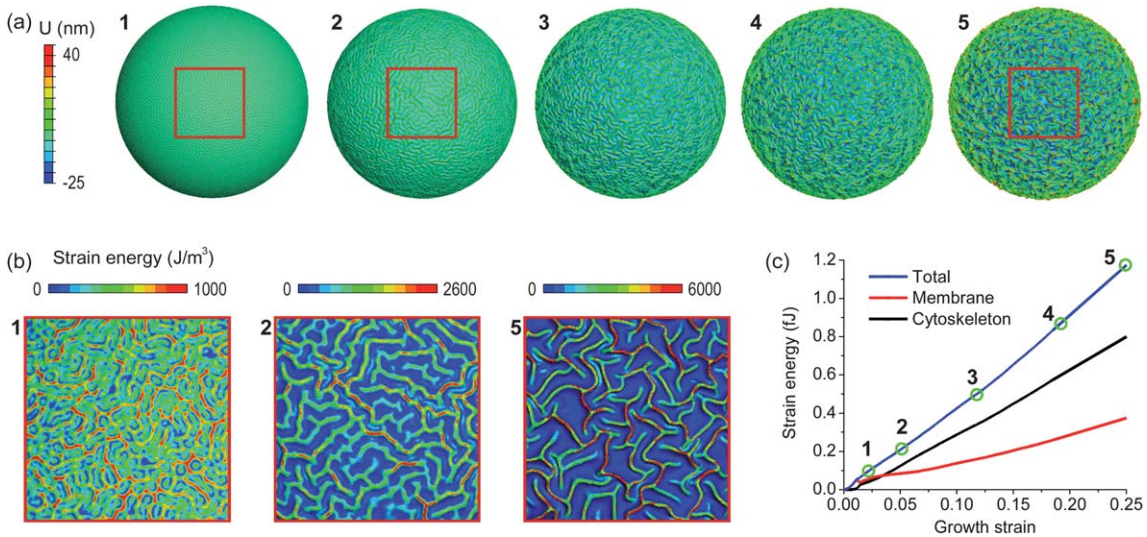


**Fig. 2** Cell membrane surface morphology evolution during membrane growth. (a) Out-of-plane displacement at different level of growth strain. (b) The corresponding elastic strain energy distribution of the membrane at 0.02, 0.05, and 0.25 growth strain (4%, 10%, and 56% area expansion, respectively). (c) Elastic strain energy of the membrane and the cytoskeleton depending on the growth strain of the membrane.

simulated amplitude agrees well with the theoretical curve given by eqn (3) for both spherical and planar membranes. At larger growth strains, the simulated amplitude is clearly greater than the theoretical estimation. As the growth strain increases, the local regular regions of sinusoidal wrinkles transformed to a more distributed labyrinth structure and the wavelength and amplitude become more distributed with peaks becoming sharper and valleys becoming wider (see Fig. 3d for typical linear traces through the wrinkle profiles). Local wavelength doubling and fold localization are also observed where the distance between two neighboring wrinkles varies greatly (see Fig. 3a, 3d and Fig. 4a). Therefore larger amplitudes are expected. To characterize the wrinkle morphology at large deformation, the apparent wavelength ($\lambda_a$, calculated as peak-to-peak or valley-to-valley distance in linear traces through the wrinkle profile) and amplitude are obtained from linear traces through the wrinkle profiles at various locations and orientations. Fig. 3e and 3f show the distribution of apparent wavelength and wave amplitude derived from linear traces at 5% and 20% growth strains. The average wavelength is ~130 nm and ~145 nm at these two strains, clearly much larger than the critical wavelength ~ 100 nm for this case. Furthermore, at large strains, the average amplitude for spherical membranes is seen to be clearly larger than that of the planar membranes because more irregularities appear in the wrinkle profiles for the spherical membrane (see Fig. 3d) as a result of more localized folds and wavelength doubling occurring in the spherical membrane. These differences are also evident in the wider distribution of wavelength and amplitude in the spherical case as shown in Fig. 3e and 3f. This is due to the curvature of the spherical membrane, indicating the curvature dependence at large strains.

Note that, uniaxial-compression induced wrinkling under large deformation has been shown to exhibit various evolutions with strain, such as a wrinkle-to-fold transition,[27] hierarchical self-similar wrinkling patterns,[28] and a period doubling bifurcation.[29] However, the large strain biaxial-stress induced wrinkling instability is largely unexplored. In our study, these results reveal the dynamic change of the membrane morphology during growth-induced biaxial deformations from small strains to large strains which are found to produce the observed surface topologies of white blood cells.

The initial wrinkle wavelength of a white blood cell, such as B cell, is computed, under an isotropic membrane assumption, to be $\sim 20t$ = 100 nm according to both simulation and theoretical prediction based on the representative material properties of the cell membrane and the cytoskeleton evolving to a wavelength of ~145nm after 50% growth strain. However, the observed wrinkle of most white blood cells has a much larger wavelength, varying from 200 to 400 nm.[5–7,9] The underestimated wavelength suggests the need for a more refined model of the cell membrane. For an isotropic shell, the bending stiffness is given by by $\kappa_b = \frac{E_m t^3}{12(1-\nu^2)}$ which for our isotropic properties gives $0.139 \times 10^{-20}$J, which is 1–2 orders of magnitude smaller than the experimentally measured value $0.13 - 4.3 \times 10^{-19}$J of lipid bilayers[21] ($1.3 \times 10^{-19}$J for red cell plasma membrane[30]). This indicates a highly anisotropic membrane behavior rather than isotropic. Note that for an isotropic material, the Poisson ratio is energetically limited to lie between $-1 < \nu < 0.5$ and our use of $\nu = 0.49$ provided a highest value for $\kappa_b$ given the reported $E_m$. Furthermore, the areal modulus of a membrane, $E_A = E_m/(1-\nu)$ is also reported to be much higher than possible for an isotropic material given the reported $E_m$ = 100kPa where $E_A = 0.12 - 0.48 \times 10^5$kPa [21](which suggests a $\nu$ of close to 1 which would be further consistent with nearly constant surface area deformation). Considering both the area compression modulus and the bending stiffness of lipid bilayers,[21] an anisotropic (transversely isotropic) model is suggested for the bilayer cell membrane with material property $E_1 = E_2 = E_3 = 100$kPa, $G_{12} = 20$kPa (in plane), $G_{23} = G_{13} = 30$kPa (out of plane), $\nu_{12} = \sim 1.0$ (in plane), $\nu_{23} = \nu_{13} = 0.0$ (out of plane) based on known material properties.[21] For example, let $\nu_{12} = 0.99$, we have a bending stiffness of $\kappa_b = 2.08 \times 10^{-19}$J, which is close to the average value of experimentally measured bending stiffness of lipid bilayers. Given this, the critical wavelength can be obtained as

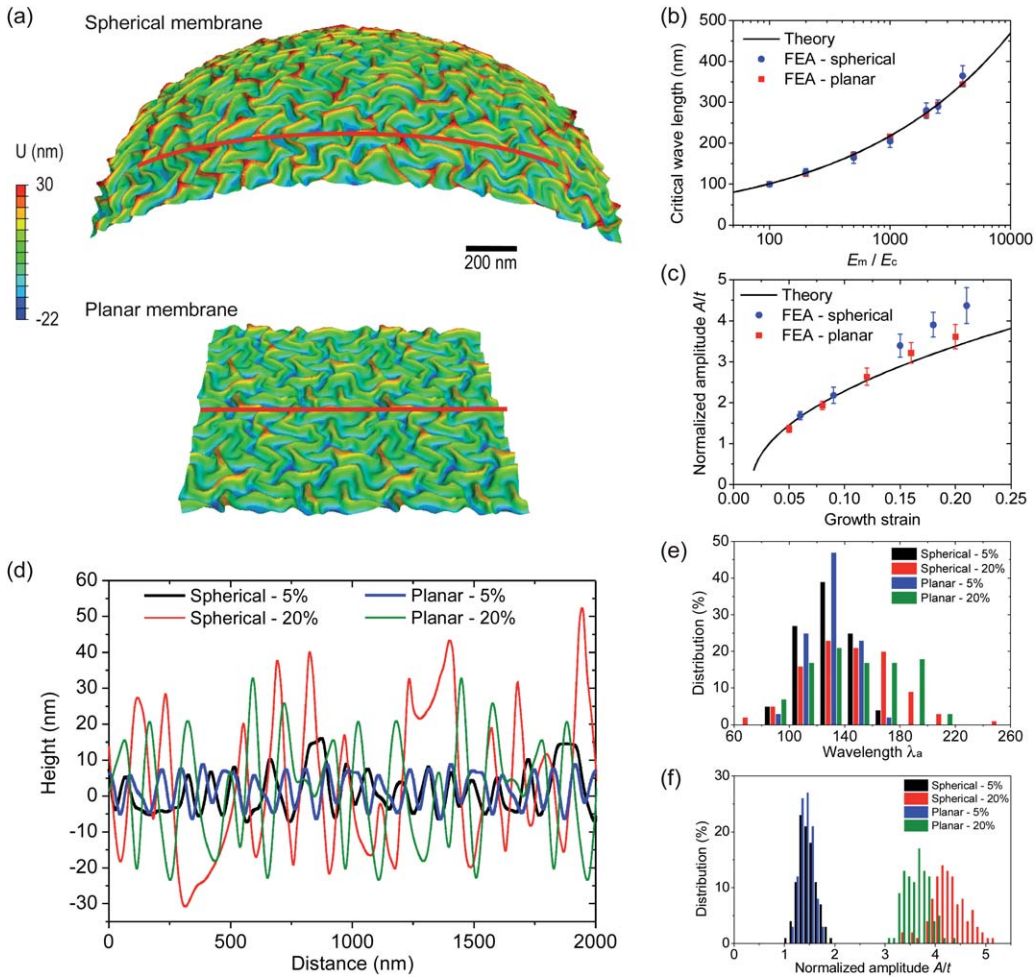


**Fig. 3** Simulated configuration of membrane surface morphology. (a) Comparison of wrinkled surface between spherical membrane and planar membrane at 20% growth strain. (b) Critical wavelength as a function of modulus ratio of the membrane and the substrate. (c) Normalized buckling amplitude as a function of growth strain. Solid lines are theoretical curves for bulking of a thin film on a compliant substrate. (d) Representative 1D wrinkle geometry characteristics of regions cut from linear traces through the wrinkle profile of the spherical membrane and planar membrane in Figure 3a at 5% and 20% growth strains. (e) Apparent wavelength distribution derived from 1D wrinkle profile of spherical membrane and planar membrane at two growth strains. (f) Apparent wave amplitude distribution derived from 1D wrinkle profile of spherical membrane and planar membrane at two growth strains.

$$\lambda_{crit} = 2\pi t\left(\frac{3E_c(1-\nu_{12}{}^2)}{E_1(1-\nu_c{}^2)}\right)^{-1/3} \quad (4)$$

The anisotropic model is implemented in the FEA simulation to examine the influence of anisotropy on the predicted surface morphology as shown in Fig. 4. Two anisotropic models are considered (where $\nu_{12} = 0.95$ and $\nu_{12} = 0.99$) and compared with the previous isotropic model. Each model exhibits a similar labyrinth pattern but the wavelength clearly differs. Since the bending energy in cell membranes is dominant in the post-buckling configurations, the isotropic model with a smaller bending stiffness underestimates the wavelength of surface wrinkles. The larger bending stiffness of the anisotropic model leads to a longer wavelength. The anisotropic model with a bending rigidity of $2.08 \times 10^{-19}$J results in an average initial critical wavelength of 270nm and a wavelength of 400nm after a growth strain of 20%, which agrees better with the SEM study of white blood cells.[6,7] This also agrees with the theoretical prediction as seen in Fig. 4e, which indicates the biaxial bending stiffness plays a significant role in the wavelength. In this case, the amplitude of wrinkles increases at a growth strain of 20% is as large as ~70 nm compared to ~20 nm for the isotropic case. The anisotropic model is capable of representing the intrinsic structural anisotropy of the cell membrane and thus provides a better prediction of the wrinkled morphology upon membrane growth.

It is also interesting to note that the surface wrinkles are stabilized through membrane-cytoskeleton linkages[31] after growth, *i.e.* a molecular velcro mechanism,[26] which makes the release of wrinkled membrane to be more complicated. To evaluate this, passive aspiration of neutrophils into micropipettes has been studied[31] and showed that a 5% membrane area expansion is obtained at small suction force, which represents the fraction of slack in the wrinkles before breaking linkages/crosslinks that hold wrinkles together. For further expansion, a greater force is required to break these linkages/crosslinks to release wrinkles. They also find a significant stiffness increase at a membrane expansion of 25–30%, indicating the wrinkles are smoothed out. More interestingly, when neutrophils are activated to expand their membrane, the force required to unravel the wrinkles is reduced significantly.[31] This enables easy and rapid morphology changes of neutrophils during phagocytosis, adhesion, or chemotaxis. Similar phenomena have been observed in the B cell where a B cell

 

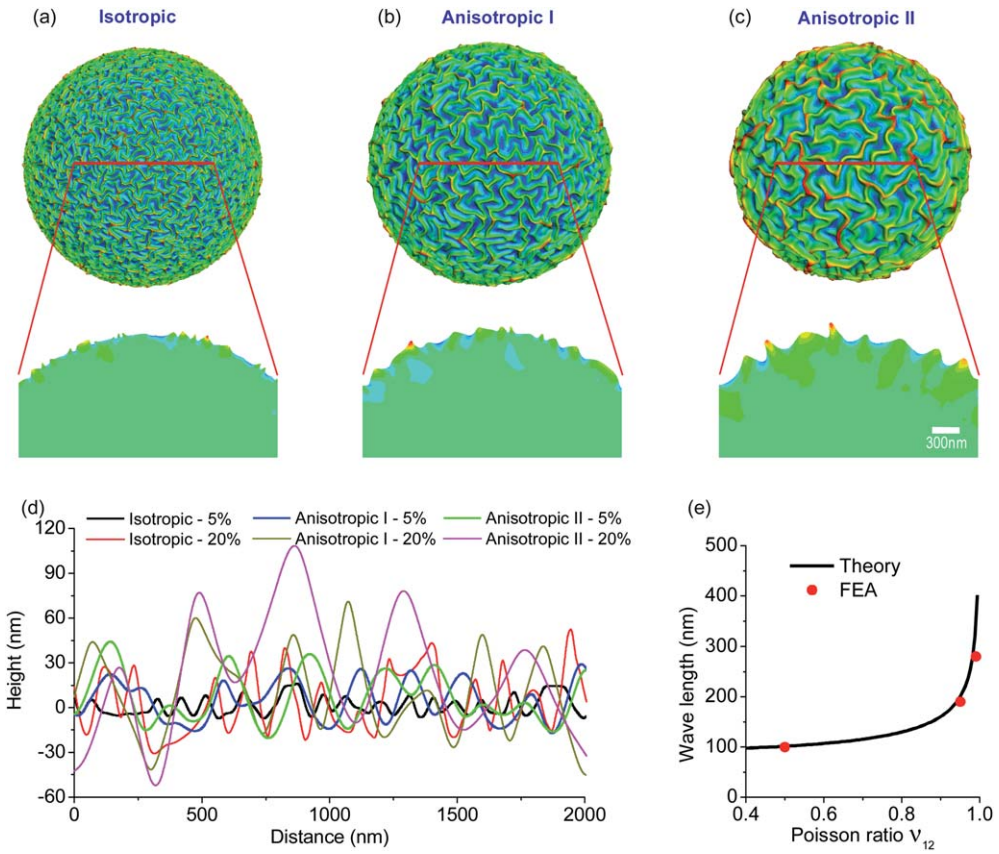


**Fig. 4** Anisotropic effects of cell membrane on the surface morphology. (a) Isotropic shell with $\nu_m = 0.5$ and $\kappa_b = 0.014 \times 10^{-19}$J, (b) Anisotropic shell with $\nu_{12} = 0.95$ and $\kappa_b = 0.4 \times 10^{-19}$J, (c) Anisotropic shell with $\nu_{12} = 0.99$ and $\kappa_b = 2.08 \times 10^{-19}$J. In the contours blue indicates valley and red indicates peak. (d) Representative 1D wrinkle geometry characteristics of linear traces through the wrinkle profile at 5% and 20% growth strains. (e) Critical wavelength as a function of in-plane Poisson's ratio of the membrane.

rapidly spreads over a target membrane 3 min after contact with membrane-bound antigen.[7]

In conclusion, buckling instabilities during membrane growth were shown to provide a physical route for the development of the labyrinth-like wrinkled morphology of a white blood cell. The wrinkle wavelength and amplitude of membranes can be quantified by the anisotropic elastic properties and the thickness of the cell membrane and the elastic properties of the underlying cytoskeleton. The microstructure of lipid bilayer suggests that the anisotropy should be considered for the cell membrane to achieve the experimentally observed wrinkle wavelength pattern and amplitude; and the evolution in the pattern with large deformation explains the sharp peaks and wide valleys to the labyrinth-like wrinkled topology. The wrinkled topology of the membrane enables large area expansion and rapid change of shape of white blood cells undergoing processes such as chemotaxis and phagocytosis. This research is expected to contribute to the understanding and modeling of physical characteristics of cellular immune response and biomedical applications where membrane mechanics plays an important role.

## Acknowledgements

This research was supported by the MRSEC Program of the National Science Foundation under award number DMR-0819762 and by the US Army Research Office through the Institute for Soldier Nanotechnologies under the Contract W911NF-07-D-0004.

## References

1 R. R. Kay, P. Langridge, D. Traynor and O. Hoeller, *Nat. Rev. Mol. Cell Biol.*, 2008, **9**, 455–463.
2 D. Traynor and R. R. Kay, *J. Cell Sci.*, 2007, **120**, 2318–2327.
3 H. P. Tingbeall, D. Needham and R. M. Hochmuth, *Blood*, 1993, **81**, 2774–2780.
4 N. Mohandas and E. Evans, *Annu. Rev. Biophys. Biomol. Struct.*, 1994, **23**, 787–818.
5 M. B. Hallett, C. J. von Ruhland and S. Dewitt, *Nat. Rev. Mol. Cell Biol.*, 2008, **9**, 662–662.
6 W. D. Marcus and R. M. Hochmuth, *Ann. Biomed. Eng.*, 2002, **30**, 1273–1280.
7 S. J. Fleire, J. P. Goldman, Y. R. Carrasco, M. Weber, D. Bray and F. D. Batista, *Science*, 2006, **312**, 738–741.
8 T. J. Kindt, R. A. Goldsby, B. A. Osborne, *Kuby Immunology*, W. H. Freeman, New York, 2007.
9 G. W. Schmidschonbein, Y. Y. Shih and S. Chien, *Blood*, 1980, **56**, 866–875.
10 N. Bowden, S. Brittain, A. G. Evans, J. W. Hutchinson and G. M. Whitesides, *Nature*, 1998, **393**, 146–149.
11 X. Chen and J. W. Hutchinson, *J. Appl. Mech.*, 2004, **71**, 597–603.
12 D. Y. Khang, H. Q. Jiang, Y. Huang and J. A. Rogers, *Science*, 2006, **311**, 208–212.
13 W. M. Choi, J. Z. Song, D. Y. Khang, H. Q. Jiang, Y. Y. Huang and J. A. Rogers, *Nano Lett.*, 2007, **7**, 1655–1663.
14 Z. Y. Huang, W. Hong and Z. Suo, *J. Mech. Phys. Solids*, 2005, **53**, 2101–2118.

15 A. Vaziri, S. F. Ahmed, G. H. Rho, K. R. Lee and M. W. Moon, *Soft Matter*, 2010, **6**, 5709–5714.
16 G. X. Cao, X. Chen, C. R. Li, A. Ji and Z. X. Cao, *Phys. Rev. Lett.*, 2008, **100**, 036102.
17 J. Yin, Z. X. Cao, C. R. Li, I. Sheinman and X. Chen, *Proc. Natl. Acad. Sci. U. S. A.*, 2008, **105**, 19132–19135.
18 L. F. Wang, C. L. Pai, M. C. Boyce and G. C. Rutledge, *Appl. Phys. Lett.*, 2009, **94**, 151916.
19 X. Chen and J. Yin, *Soft Matter*, 2010, **6**, 5667–5680.
20 M. Dao, C. T. Lim and S. Suresh, *J. Mech. Phys. Solids*, 2003, **51**, 2259–2280.
21 D. Boal, *Mechanics of the Cell*, Cambridge University Press, Cambridge, UK, 2002.
22 G. T. Charras, B. A. Williams, S. M. Sims and M. A. Horton, *Biophys. J.*, 2004, **87**, 2870–2884.
23 P. Miller, L. L. Hu and J. L. Wang, *J. Mech. Behav. Biomed. Mater.*, 2010, **3**, 268–277.
24 R. M. Hochmuth, C. A. Evans, H. C. Wiles and J. T. McCown, *Science*, 1983, **393**, 101–102.
25 P. W. Kuchel and G. B. Ralston, *Schaum's Outline of Theory and Problems of Biochemistry*, McGraw-Hill, New York, 1987.
26 M. B. Hallett and S. Dewitt, *Trends Cell Biol.*, 2007, **17**, 209–214.
27 L. Pocivavsek, R. Dellsy, A. Kern, S. Johnson, B. H. Lin, K. Y. C. Lee and E. Cerda, *Science*, 2008, **320**, 912–916.
28 K. Efimenko, M. Rackaitis, E. Manias, A. Vaziri, L. Mahadevan and J. Genzer, *Nat. Mater.*, 2005, **4**, 293–297.
29 F. Brau, H. Vandeparre, A. Sabbah, C. Poulard, A. Boudaoud and P. Damman, *Nat. Phys.*, 2011, **7**, 56–60.
30 E. A. Evans, *Biophys. J.*, 1983, **43**, 27–30.
31 M. Herant, V. Heinrich and M. Dembo, *J. Cell Sci.*, 2005, **118**, 1789–1797.

 